Tidal impacts on downstream hydraulic geometry of a tide-influenced delta

Xiaomei Ji[1,2] · Wei Zhang[1,2] 🆔

Abstract

Variations in river hydraulic geometry (HG) are of fundamental importance to fluvial geomorphological research and catchment management. In tide-influenced river deltas, channel geometry displays a mixed scaling behavior since the channel forming discharge is of both tidal and river origins. This study aims to map the tidal signature on delta morphology in the Pearl River Delta (PRD) channel network. The model results of a 2D numerical model are used to analyze the spatial variations of river and tidal discharges and their relations with representative channel geometry throughout the delta. Downstream HG of the distributary channels in the PRD features distinct characteristics in three zones. The transition points in morphology, which splits the delta into river- and tide-dominated parts, coincide with those in the mean flow velocity, the ratio of maximum tidal discharge amplitude (MTDA) to fluvial discharge. The ratio of MTDA to river discharge scales with bifurcation order. The water level setup created by non-linear tidal and fluvial interactions affects the discharge division at tidal bifurcations. In general, the net tidal impact is to attenuate the inequality in discharge division in the PRD. The tide is non-negligible in the cross-sectional morphology and plays a decisive role in the formation of the river channel in the seaward portion of the delta.

1 Introduction

Downstream hydraulic geometry (HG), as developed by Leopold and Maddock (1953), is used to describe the spatial variations in river hydraulics along river networks at a characteristic reference flow such as the mean annual discharge (Lee and Julien 2006). It can be expressed via a set of empirical power law relations between the water discharge and the channel geometric properties (e.g., channel width, mean depth, mean flow velocity; Leopold and Maddock 1953).

Variation in river hydraulic geometry is fundamentally important to fluvial geomorphological research and catchment management because of its influence on physical habitats, water temperature, nutrient and pollutant fluxes, sediment transport rates, biodiversity, and ecosystem services (Statzner et al. 1988; Maddock 1999). In recent studies, hydraulic geometry relationships have been used for planning tidal wetland restoration projects (Williams et al. 2002), modelling sediment transport (Goodwin 2004), estimating habitat alteration due to water abstraction (Snelder et al. 2011; Miguel et al. 2016), modelling nutrient fluxes (Dupas et al. 2013), modelling river temperature (Beaufort et al. 2016), or modelling streambed hydraulic conductivity (Stewardson et al. 2016). Lamouroux et al. (2017) also identified hydraulic geometry as the key for integrating hydraulic information in large-scale environmental flow studies.

In tide-influenced deltas, tides exert a strong control on delta morphology (Hoitink et al. 2017). Tides penetrate into the channel networks, alter the hydrology and sediment transport of deltaic channels (Godin 1985; Savenije 2012), and act to reshape the delta morphology. Morphologically, tides tend to widen delta distributary channels (Langbein 1963; Wright

et al. 1973). Myrick and Leopold (1963) found that a tidal channel changed more rapidly in width and less rapidly in depth as discharge changed downstream than did a terrestrial channel. Sassi et al. (2012) studied the Mahakam Delta in Indonesia with a hydrodynamic model and proposed that channel widening occurred when the tidally driven discharge exceeded the fluvial discharge. Nienhuis et al. (2018) provided a simple method to predict the magnitude of deltaic channel widening. Besides, non-linear interactions between tides and river discharge lead to flow changes within channels and a more uniform distribution of discharge across channels (Buschman et al. 2010; Sassi et al. 2011). Systematic variation of the tidal range may lead to a cyclic variation in water discharge distribution at bifurcations, affecting the hydraulic geometry relations (Hoitink et al. 2017).

Traditionally, the tidal prism or peak tidal discharge is used to quantify the tidal impacts on a delta (Friedrichs 1995; Rinaldo et al. 1999; Syvitski and Saito 2007; D'Alpaos et al. 2010). However, to evaluate the degree to which channel morphology is affected by the tidal fluctuation throughout the distributary channel network, a more reliable and effective set of metrics is needed. Hydraulic geometry provides a synoptic insight into the dominant controls on the morphology of delta channels. The inclusion of tides in the HG concept (Williams et al. 2002) and the application to the delta channel network will quantify the extent to which tides impact the variation of river discharge over the delta network (Dodov and Foufoula-Georgiou 2004; Sassi et al. 2012). Furthermore, the traditional hydraulic geometry concept is improved by replacing the tidal prism with the maximum tidal discharge amplitude (MTDA). The latter is based on the sum of the major tidal discharge amplitudes, which describes the tidal discharge more precisely than the former. The bifurcation number is also introduced to HG for the situations where tidal characteristics are not available.

The Pearl River Delta (PRD; Fig. 1), located at the northern reach of the South China Sea, is one of the world's most complicated river networks and deltaic drainage systems. Intensive anthropogenic activities, such as sand excavation (Luo et al. 2007), land reclamation (Chen et al. 2010), dam construction (Zhang et al. 2017), and channel dredging (Yuan and Zhu 2015), caused changes in the channel geometry as well as in the river hydraulics. Jia et al. (2002) discussed the changes of the hydraulic geometry at the delta apex of the PRD in recent decades. The influence of human-induced river channel incision on river hydraulics in the PRD was evaluated by comparing the stage-discharge curves from different years (Lu et al. 2007; Zhang et al. 2015). Although variations of the hydraulic geometry in the PRD have been widely documented, they are still largely unexplained, especially that the effect of tides is generally ignored.

This study aims to quantify the tidal signature on delta morphology by applying the improved hydraulic geometry concept to the tidally influenced PRD. First, a description is given of the PRD channel networks and the hydrodynamic model is presented in Section 2. Next, in Sections 3.1 and 3.2, the spatial variation of the representative channel geometry from the delta apex to the coast is described. Then, the hydrodynamic processes are mapped onto the delta network in Section 3.3. Afterwards, the hydraulic geometry framework for channel networks affected by tides is introduced and the mechanisms governing river discharge division are discussed in Section 4. And in Section 5, this study is finalized with conclusions.

2 Study area and numerical model

2.1 The Pearl River Delta channel network

The Pearl River is the second largest river in China (only surpassed by the Yangtze River) and 13th largest river in the world in terms of annual mean water discharge which amounts to over 3×10^{11} m^3 (Pearl River Water Resources Commission 1991). It extends from Yunnan Province in Southwest China to Guangdong Province before pouring into the South China Sea with a total length of 2214 km. The Pearl River system is a compound water system including three principal rivers (Fig. 1): the West River (77.9% of the total basin area), the North River (10.3%), and the East River (6.0%). These rivers branch and intertwine, forming a irregularly distributed, fan-shaped delta, the Pearl River Delta (PRD). The PRD is considered as one of the world's most complicated river networks, with the density of channel length per unit area at 0.68–1.07 km/km^2 (Chen and Chen 2002).

Geographically, waters from the West River and the North River enter the delta network through the apex bifurcation at Sixianjiao (Fig. 1). The contributions of the West River, the North River, and the East River to the PRD in terms of discharge are 77%, 15%, and 8%, respectively (Zhang et al. 2015). The West River and the North River are the most important rivers in the PRD. All of these tributaries debouch into the South China Sea through eight outlets, namely Yamen, Hutiaomen, Jitimen, Modaomen, Hengmen, Hongqimen, Jiaomen, and Humen from west to east (Fig. 1).

The tides in the Pearl River Estuary mainly come from the Pacific oceanic tidal propagation through the Luzon Strait, with a gradual increase in the tidal range and reaches a maximum near the river outlets (Mao et al. 2004). The estuary is a microtidal one with an average spring tidal range of 0.86–1.60 m (Zhang et al. 2010). The tides are characterized as a semidiurnal mixed tidal regime with daily inequality in both range and time. M_2 is usually the dominant tidal constituent, followed by K_1, O_1, and S_2 (Zhao 1990; Mao et al. 2004; Ji and Zhang 2019).
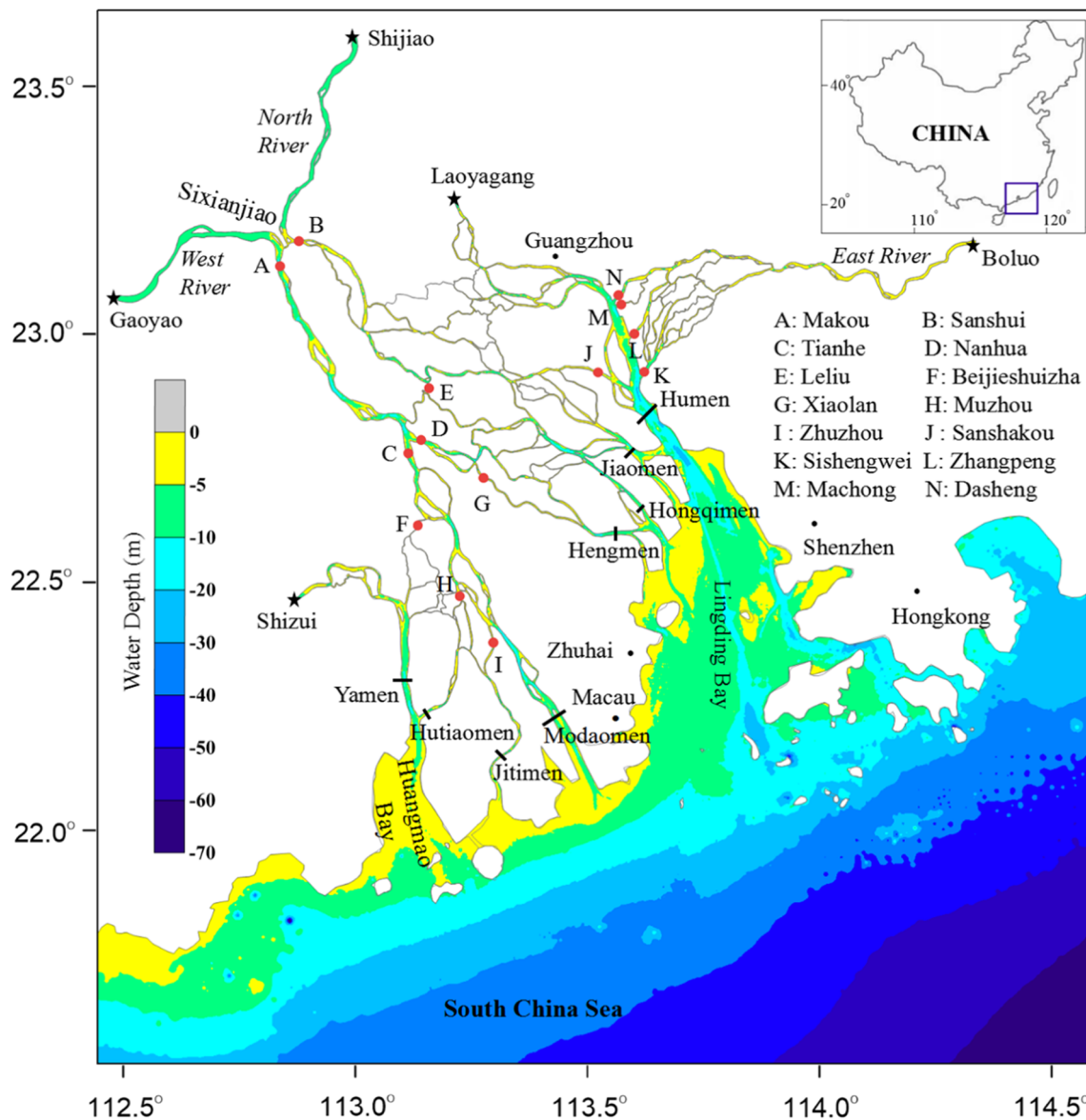
Fig. 1 Bathymetry of the Pearl River Delta and its river networks. The inset shows the location of the delta. The black short lines show the positions of the eight outlets. The black stars represent the hydrological stations for upstream boundaries. The red circles represent the hydrological stations for validation

2.2 Hydrodynamical model

An unstructured mesh, finite element model driven by the tides and river discharges (Ji and Zhang 2019) was applied to simulate the hydrodynamics in the PRD. A mesh of 55,454 nodes and 56,911 quadrilateral or triangular elements is employed to represents the bathymetry and geometry of the river networks and the coastal waters, with the model grid size ranging from 50 to 2000 m (Fig. 2). The bathymetry and geometry of the river networks and the coastal waters were obtained from the navigational charts and topographic surveys made in 1999. Daily averaged river discharge series obtained from Gaoyao, Shijiao, Laoyagang, Boluo, and Shizui hydrological stations

(positions shown in Fig. 1) were used to force the model at the upstream boundary. Tides from a triply nested ocean circulation model of the China Seas (Ji et al. 2011) were used to force the model at open boundaries extended to the 30 m water depth.

The Manning's roughness coefficient is 0.03 for the upstream channels and decreases to 0.015 for the downstream channels. The horizontal mixing scheme suggested by Smagorinsky (1963) is used to compute the horizontal eddy viscosity and diffusivity coefficients. In the meanwhile, the wetting and drying algorithm is implemented by moving the nodes on the boundaries to guarantee that the water depth always remains positive over the whole domain. The critical depth is set to 0.1 m.

Fig. 2 Model mesh for the full domain with inserts showing close-up of the grids
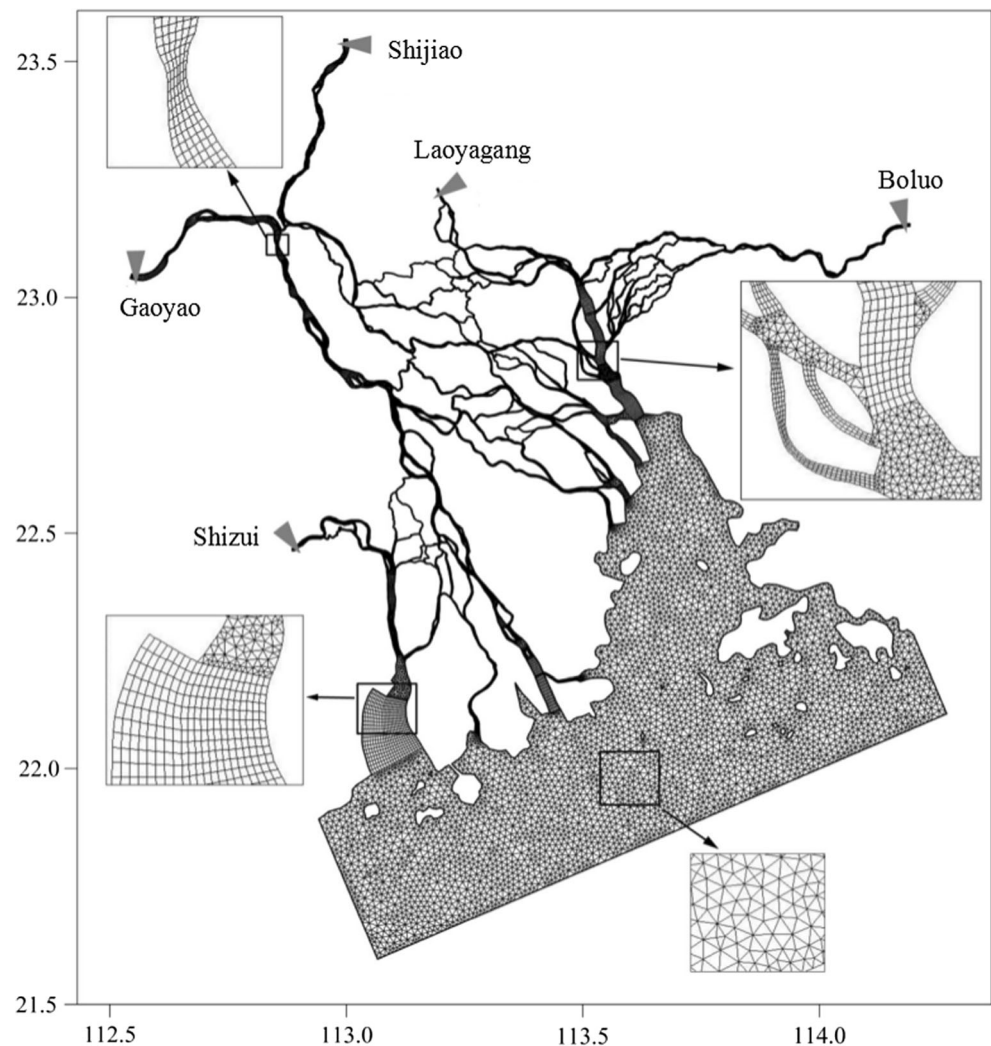
The model performance was evaluated by comparing model results with water elevation and discharge time series at 14 hydrological stations in dry season and 8 stations in wet season. The model skill score (SS) is calculated as the ratio of model error to variability in observational data (Maréchal 2004; Allen et al. 2007).

$$SS = 1 - \frac{\sum(X_{\mathrm{mod}} - X_{obs})^2}{\sum\left(X_{obs} - \overline{X}_{obs}\right)^2} \qquad (1)$$

Figure 3 displays the results of model validation of water level and discharge in the dry season. It can be seen that the performance levels mainly fall into the excellent and very good categories. More details of the model implementation and performance can be found in Ji and Zhang (2019).

When different factors are investigated by numerical experiments, non-linear interactions between the factors need to be considered. A pioneering study in this area is that of Stein and Alpert (1993). They designed a methodology for factor

separation in numerical simulations, of which the key element is the derivation of interaction effects. Their approach has been highly influential and used in a large number of studies (e.g., Braconnot et al. 1999; Claussen et al. 2001; Hogrefe et al. 2004; van den Heever et al. 2006; Torma and Giorgi 2014). Here, the factor separation analysis (Stein and Alpert 1993) was applied to the time series of water discharge. The model was run under the following three forcing conditions. In the river-and-tide case, the model configuration is the same as described above. In the tide-only case, the model is forced with tides at the downstream boundaries, whereas radiative boundary condition is imposed at suitable upstream locations. In the river-solely case, the model is forced with river discharges at the upstream boundaries and the downstream boundaries are set to equilibrium water level.

3 Channel morphology and hydrodynamics

Figure 4 shows the channel centerlines of the Pearl River Delta channel network. The centerlines are obtained as the

Fig. 3 The results of model validation of water level (left) and discharge (right) over the PRD in the dry season
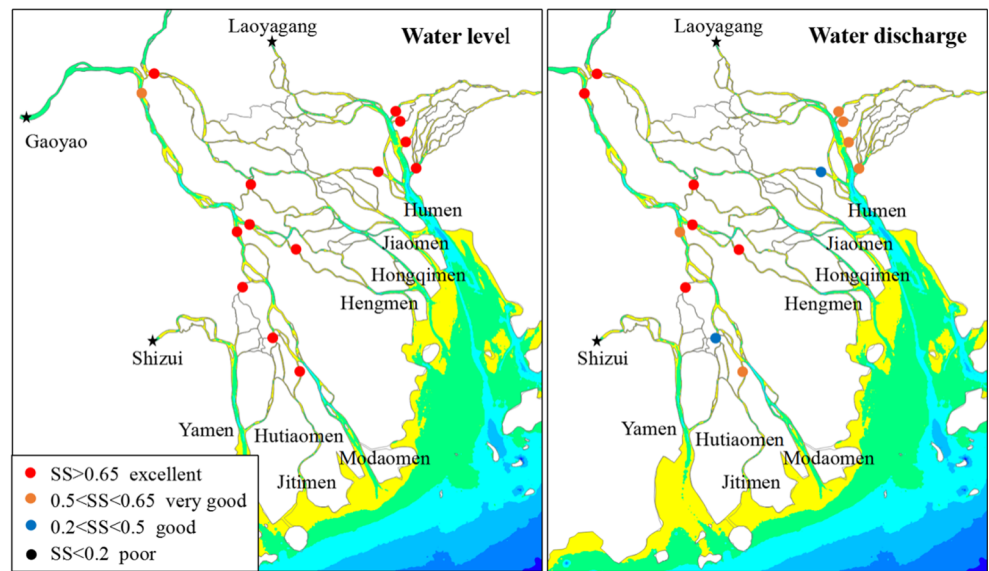
mean location line between the banklines, which are generated from maps, the bathymetric surveys, and the remote sensing images. Representative cross sections are chosen near the tidal bifurcations. At each cross section, the width and mean water depth are computed and discharges and water levels obtained from the hydrodynamic model are stored. The hydraulic geometry analysis is based on these cross sections.

Fig. 4 Centerlines of the Pearl River Delta channel network. Dashed lines indicate arcs through the main bifurcations, with a constant radial distance to the delta apex Sixianjiao. s is the channelized distance from the apex and L is the attained distance to the coast along the longest distributary
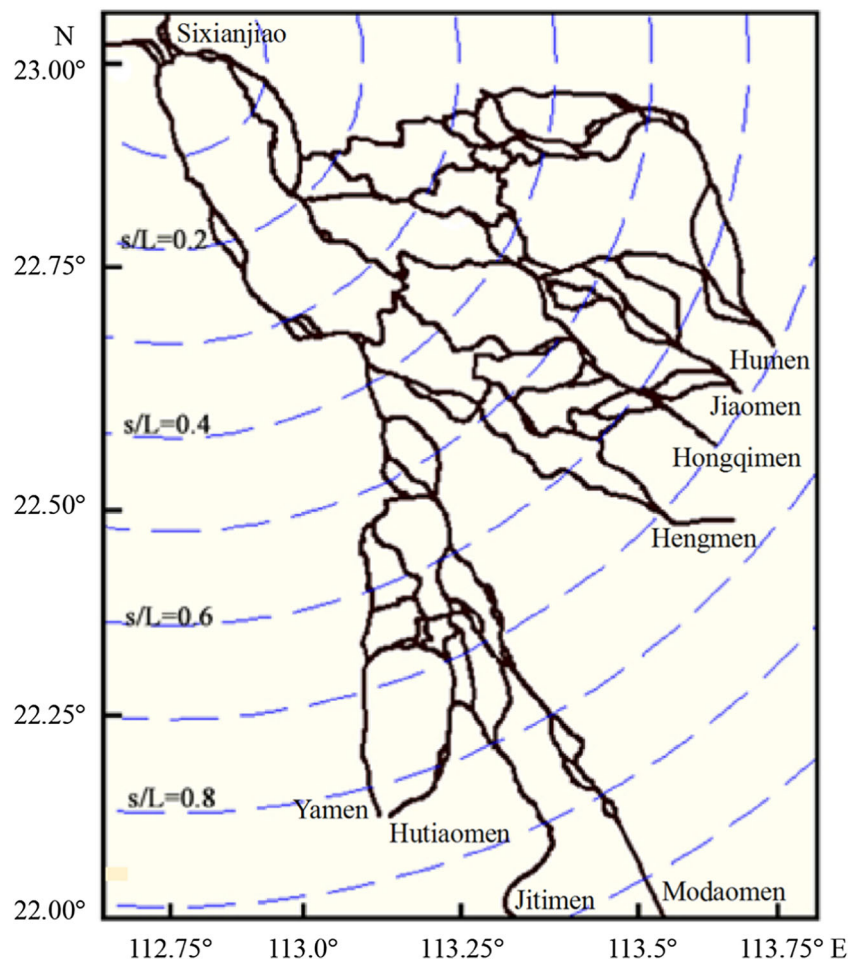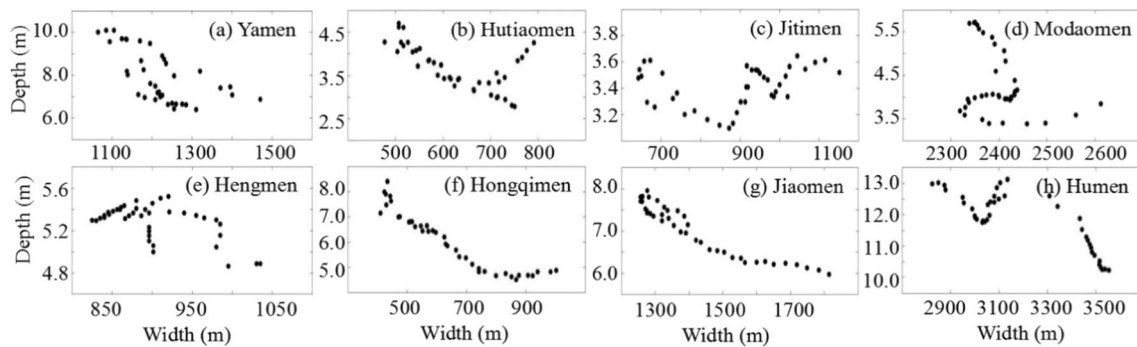
Fig. 5 Mean water depth as a function of channel width for the eight distributary outlets of the PRD, from west to east (positions of the outlets are shown in Fig. 1). **a** Yemen. **b** Hutiaomen. **c** Jitimen. **d** Modaomen. **e** Hengmen. **f** Hongqimen. **g** Jiaomen. **h** Humen

3.1 Channel morphology at river outlets

The channel width and mean water depth are computed at the river outlets (the interval of each computational cross section at the channel is about 100 m). Figure 5 shows mean depth as a function of channel width for the eight distributary outlets of the PRD, from west to east (positions of the outlets are shown in Fig. 1). The mean water depth is cross-sectionally averaged water depth obtained from the hydrodynamic model. At the Yamen, Hongqimen and Jiaomen outlets, the mean water depth is inversely correlated to width (Fig. 5a, f, g). The inverse relation weakens seaward, because the downstream channels are used for navigation and are subject to continuous dredging activities. These three distributaries demonstrate a clear relationship between channel depth and width, though there are some variabilities across the channels.

At the Hutiaomen, Jitimen, Modaomen, Hengmen, and Humen outlets, the negative correlation between the mean water depth and the width is not significant (Fig. 5b, c, d, e, h), due mainly to the complexity of the topography and the impacts of intensive human interventions on channel

morphology. Luo et al. (2007) estimated that more than 8.7×10^8 m^3 of sand were excavated in the PRD from 1986 to 2003, resulting in obvious riverbed downcutting and channel volume increment. The channel geometry and the river hydraulics have been dramatically changed due to the rapid downcutting (Lu et al. 2007).

3.2 Channel morphology along the channel network

A representative channel geometry is computed as the average depth and width over all channels at a given radial distance from the delta apex and the cross-sectional area and aspect ratio derived from those parameters. Variability across the channels is more apparent near the delta apex than near the coast, because the number of averaged channels increases from the apex to the coast. Figure 6 displays the spatial development of the representative channel geometry from the delta apex toward the coast, as a function of the normalized along-channel distance, s/L, where s represents the along-channel distance from the delta apex and L is the distance to the coast along the longest distributary.

Fig. 6 Spatial variation of the representative channel geometry from the delta apex to the coast, computed as the mean over all distributaries. The shaded area indicates one standard deviation. Solid lines indicate the best-fit lines. Red diamonds denote the cluster means, binned as a function of s/L. **a** Depth (m). **b** Width (m). **c** Area (m^2). **d** Width to depth ratio
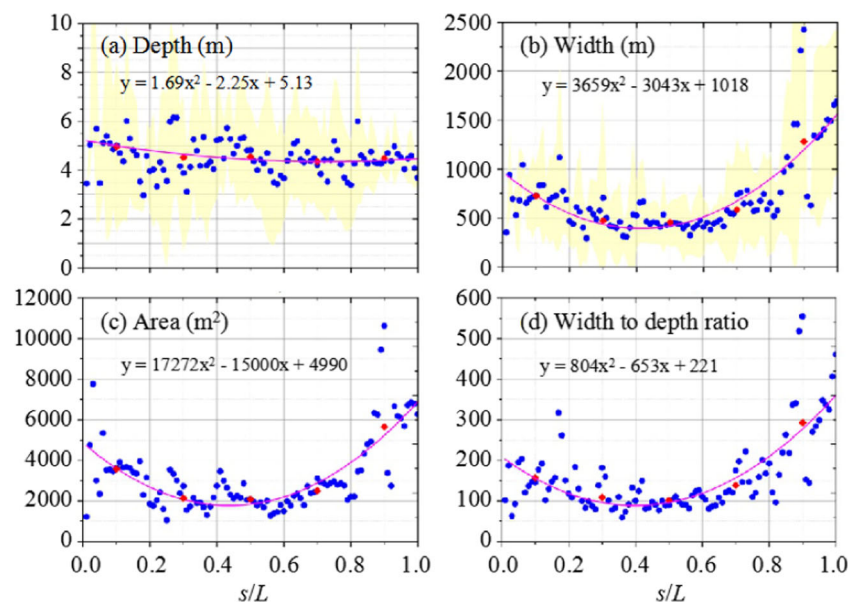
The representative channel depth exhibits a decreasing trend closer to the coast, with an average value of about 5.0 m around the delta apex and about 4.5 m near the coast (Fig. 6a). The representative channel width decreases from 1000 to 500 m over the first 10% of the total radial distance. Within a distance roughly between 30 and 50% of the total radial distance between the apex and the coast, the width varies little around a mean value of 500 m. In the remainder of the delta, the width features an increasing trend toward the coast (Fig. 6b). The representative channel area decreases from the delta apex up to about the region bounded by an arc with a radius of about 30% of the total radial distance to the apex. Within a distance roughly between 30 and 60% of the total radial distance between the apex and the coast, the area oscillates around 2000 m^2 and increases seaward beyond the 60% arc (Fig. 6c). The representative aspect ratio decreases inapparently over the first 30% of the total radial distance, and oscillates around a constant value of 100 between 30 and 60% of the total radial distance, and increases seaward in the remaining part (Fig. 6d).

The representative channel geometry presents three well-defined regions. In the landward 30% of the PRD, the scaling behavior of the representative channel geometry coincides with the scaling observed in river deltas (Edmonds and Slingerland 2007). In the seaward 40% of the delta, the representative channel geometry resembles that of funnel-shaped estuarine channels (Davies and Woodroffe 2010), reflecting the importance of the tidal discharge relative to the river discharge in channel forming processes (Fagherazzi and Furbish 2001). The PRD reveals a large transition area between the river-dominated and tide-dominated domains (Fig. 6).

3.3 Channel hydrodynamics

In tide-influenced river deltas, channel geometry shows a mixed scaling behavior between that of tidal channel and river networks, because the channel forming discharge is of both tidal and river origins (Sassi et al. 2012). Thus, at each cross section, the water discharge Q can be decomposed into two parts:

$$Q = Q_R + Q_T \qquad (2)$$

where Q_R and Q_T are the river and tidal discharges, respectively. Here the tidal discharge Q_T is defined as follows:

$$Q_T(t) = \sum_j Q_j(t) \qquad (3)$$

$$Q_j(t) = P_j(t)\cos\left(ij\omega_j t + \varphi_j\right), j = 1/14, 1, 2, 4 \qquad (4)$$

where the subscripts 1/14, 1, 2, and 4 denote fortnightly, diurnal, semidiurnal, and quarterdiurnal tidal species, respectively; P_j, ω_j, and ϕ_j represent the tidal discharge amplitude, the angular frequency, and the phase corresponding to the above four tidal species; and i stands for the imaginary unit.

The tidal species here denotes a group of tidal constituents with frequencies corresponding to a frequency band, as opposed to a unique frequency (Jay 1997).

At a given time, the maximum tidal discharge amplitude (MTDA) P can be expressed as the sum of the tidal discharge amplitude of the four species:

$$P = \sum_{j=1/14,1,2,4} P_j \qquad (5)$$

In tidal systems, the tidal prism defined as the volume of water between mean high tide and mean low tide is used instead of a discharge with a constant frequency of exceedance (Friedrichs 1995; Rinaldo et al. 1999; D'Alpaos et al. 2010). Here the maximum tidal discharge amplitude is considered to be a surrogate of the maximum astronomical tidal prism. Amplitudes of fortnightly, quarterdiurnal, semidiurnal, and diurnal fluctuations are generated by applying continuous wavelet transform to the modelled water discharge and water level time series obtained at the selected cross sections near tidal bifurcations in the delta. The numerical model is used to simulate scenarios include high and low river discharge input, with and without the tidal forcing. Model runs span 2 months, and all quantities are averaged over the entire simulation period.

Figure 7 displays the spatial distribution of river discharge Q_R, maximum tidal discharge amplitude P, the ratio of tidal to fluvial discharge P/Q_R, and mean flow velocity U for locations of the selected cross sections. The scatter increases seaward because the flow is obtained at a limited number of cross sections, which span a confined range of the spatial extent of the delta. Q_R shows a seaward decrease in magnitude (Fig. 7a). In the region bounded by an arc with a radius of about 40% of the total radial distance to the apex, the decrease trend is more apparent than the remainder of the delta. The decrease in Q_R with distance to the delta apex reflects the partitioning of river discharge at the bifurcations. Conversely, the landward increase in P over the first 40% of the total radial distance (Fig. 7b) reflects the combination of tidal discharges at the bifurcations. In the remainder of the delta, P decreases landward since the tidal action is getting stronger seaward (Fig. 7b).

From Fig. 7c, it can be seen that the ratio between MTDA and river discharge P/Q_R increases seaward; the tidal impact on river channels becomes stronger as the distance from the delta apex increases. Over the first 40% of the total radial distance, the ratio shows apparent increment and reaches about 1.0 which indicates that the maximum tidal discharge amplitude is comparable to the river discharge at $s/L = 0.4$. Within a distance roughly between 40 and 70% of the total radial distance, the ratio is relatively steady. In the remainder of the delta, the ratio increases slightly, suggesting the strengthened tidal dynamics.

Mean flow velocity U, defined as the ratio between Q and A, depicts a decrease in magnitude (Fig. 7d). Over the first 35% of

Fig. 7 Spatial distribution of river discharge Q_R (**a**), maximum tidal discharge amplitude P (**b**), the ratio of tidal to fluvial discharge P/Q_R (**c**), and mean flow velocity U (**d**) for locations of the selected cross sections. Solid lines indicate the best-fit lines. Diamonds denote the cluster means, binned as a function of s/L
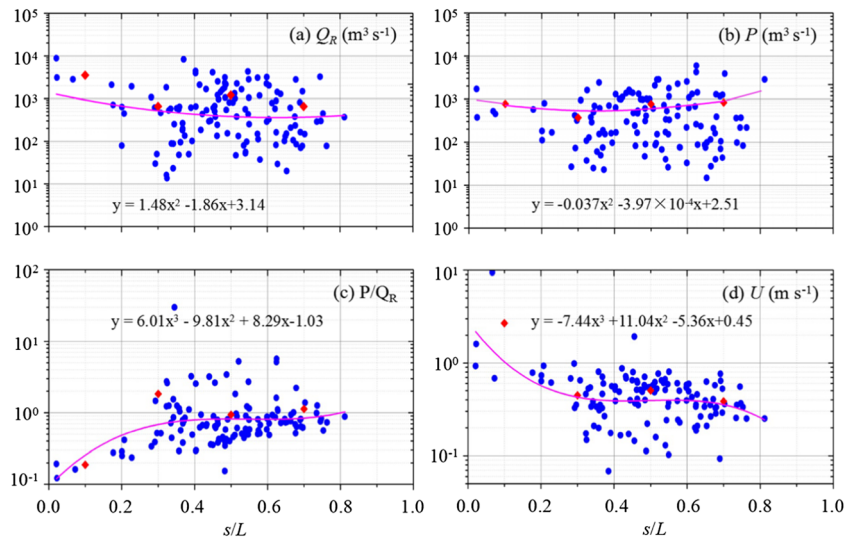
the total radial distance, the mean flow velocity shows apparent decrements; within a distance roughly between 35 and 70% of the total radial distance, the velocity is relatively steady; and in the remainder of the delta, the velocity decreases.

It is worth noting that the location of the break point in the hydrodynamics coincides fairly well with the location of a shift in scaling behavior of the channel network, separating the PRD into a river delta part, a transition part, and a coastal margin featuring funnel-shaped estuaries.

4 Tidal impacts on HG relations

In the delta channel networks, bifurcations play a key role in determining the water and sediment division in the down-stream distributary channels (Sassi and Hoitink 2013). Due to the impacts of tides and river-tide interaction, variations of discharge division at a bifurcation will further affect the downstream hydraulic geometry relations.

4.1 Relation between river discharge and MTDA

We examine the tidal influence on hydraulic geometry relations by quantifying the tidal impact on the Pearl River

Delta (PRD) channel networks. We first separate the river discharge and tidal discharge and then analyze (i) the relation between the maximum tidal discharge amplitude (MTDA) and the river discharge and (ii) the relation between the cross-sectional area and the discharges. Figure 8 a presents the relationship between the maximum tidal discharge amplitude and the river discharge under high and low flow conditions. The best-fit lines in the log-log plot show obvious linear relation, which indicates that channels conveying high river discharge also convey a high tidal discharge. Thus, Q_R can be expressed as a power law of the form

$$Q_R = cP^d \tag{6}$$

where c and d are two coefficients.

Contributions of the four tidal species (i.e., diurnal, semi-diurnal, quarterdiurnal, and fortnightly tides) to the maximum tidal discharge amplitude P are separated from the model results under high flow condition using wavelet analysis. The contributions are all positively correlated with the river discharge conveyed by the channel (Fig. 8b), with similar slopes for all species. The semidiurnal species feature the largest tidal prism, followed by the diurnal, quarterdiurnal, and fortnightly species.

Fig. 8 **a** Maximum tidal discharge amplitude P as a function of river discharge Q_R. The solid lines indicate the best-fit lines in log space for low and high flow conditions. R^2 is the goodness of fit. **b** Diurnal (P_1), semidiurnal (P_2), quarterdiurnal (P_4), and fortnightly ($P_{1/14}$) contributions to P as a function of Q_R
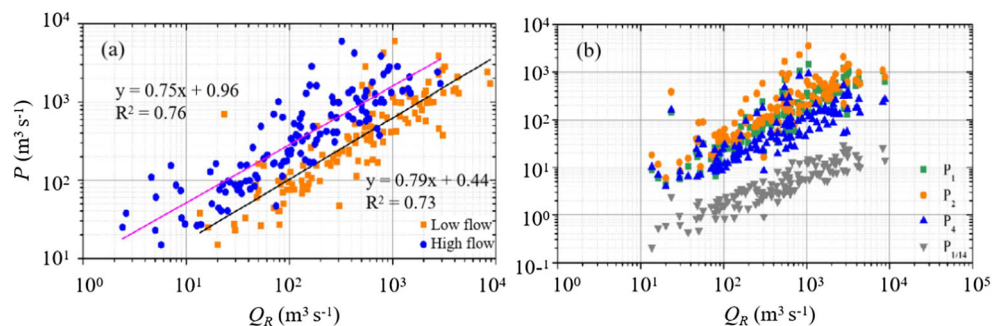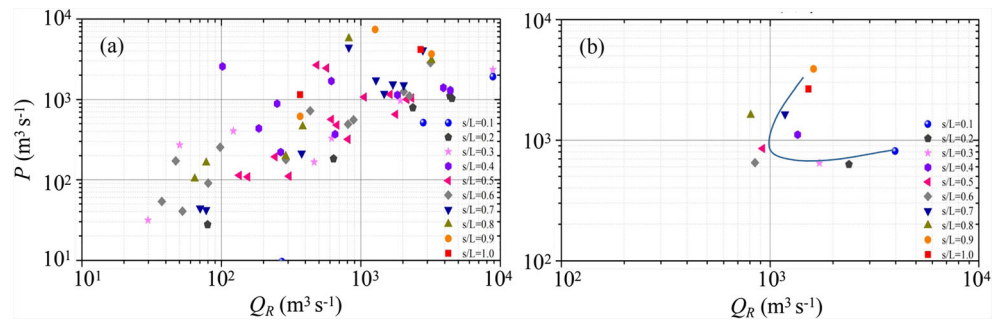
Fig. 9 **a** Maximum tidal discharge amplitude P as a function of river discharge Q_R for simulations with high flow, but color coded by s/L values, as indicated. **b** Same as **a** but binned and averaged over s/L

The variations of the relation between MTDA and river discharge along the channel network from the delta apex to the outlets are shown in Fig. 9. Figure 9 a demonstrates the same data as Fig. 8a, for simulations with high flow, but coded for incremental ranges of s/L. Figure 9 a indicates that channels conveying low river discharge also convey a low tidal discharge. Figure 9 b expresses the same data as Fig. 9a but binned and averaged over s/L. It can be seen from Fig. 9b that there is transition point at $s/L = 0.5$~0.6, separating the delta into three parts, the river-dominated zone, the transitional zone, and the tide-dominated zone, similar to that discussed in Sections 3.2 and 3.3.

4.2 Linking tidal hydrodynamics to channel morphology

In their simplest form, hydraulic geometry relationships can be fitted to power laws (Leopold and Maddock 1953):

$$A = aQ^b \tag{7}$$

where A is channel cross-sectional area at instantaneous discharge Q. Parameter a is the hydraulic geometry coefficient,

and b is the corresponding exponent. Log transformation of variables is frequently used to linearize Eq. (7).

Consider the hydraulic geometry relation of the area of a channel network in morphological equilibrium that conveys both river and tidal discharges and use the maximum tidal discharge amplitude P instead of tidal discharge Q_T:

$$A = a(Q_R + P)^b \tag{8}$$

If $P/Q_R < 1$, retaining the first two terms of the binomial series expansion of A yields the following:

$$A \approx a\left(1 + b\frac{P}{Q_R}\right)Q_R^b = aQ_R^b + abPQ_R^{b-1} \tag{9}$$

Considering Eq. (6), Eq. (9) can be rewritten as follows:

$$A \approx ac^b\left(1 + \frac{b}{c}P^{1-d}\right)P^{db} \tag{10}$$

Equation (10) shows the form of the relation between A and P in tidally influenced deltas.

Fig. 10 Log-log plots of the cross-section area and the discharge conveyed by the channel, using **a** the river discharge Q_R, **b** the maximum tidal discharge amplitude P, **c** the total discharge $Q_R + P$, and **d** $(\phi + 1)Q_R$, color coded by s/L values. Full lines represent the best-fit line through the data. R^2 is the goodness of fit. The dashed line indicates the line of equal values
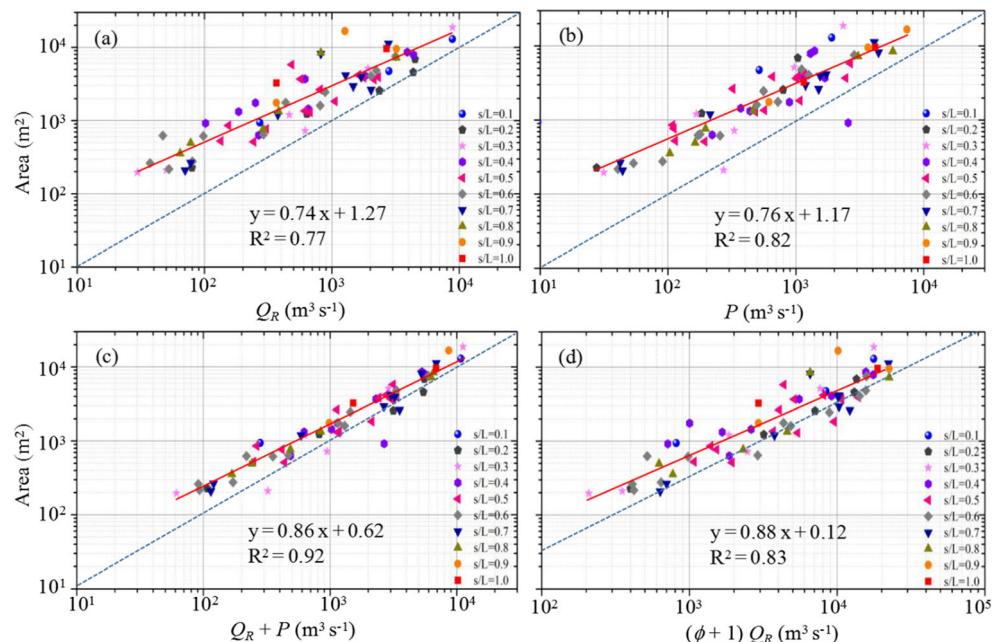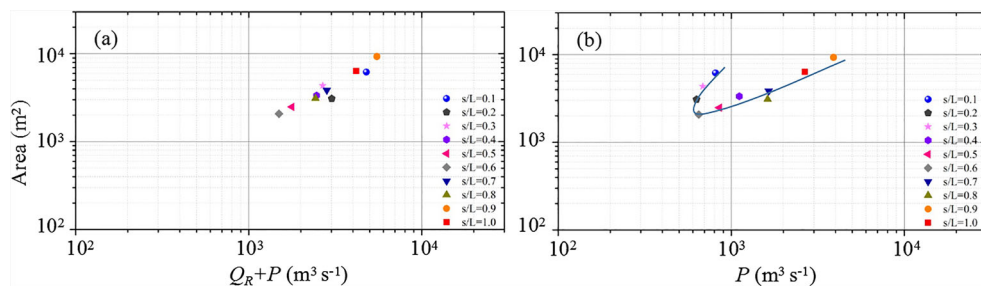
Fig. 11 Cross-section area as a function of **a** the total discharge $Q_R + P$ and **b** the maximum tidal discharge amplitude P, binned and averaged over s/L, color coded by s/L values

As it can be seen from Fig. 7c, the ratio between MTDA and river discharge P/Q_R changes rapidly in the upstream reach of the channel network, while the ratio is relatively steady in the middle stream area. This might be because the river channels bifurcate and rejoin and generate intertwined channel networks in the middle reach. The river channels keep bifurcating, and the discharge conveyed by the branch channels keep reducing while the anabranch channels convey the discharges from different upstream channels. The river discharge reduces in the downstream direction when the number of branches increases (Edmonds and Slingerland 2007). The tidal discharge is also dividing and rejoining while propagating upstream in the channels. Thus, it can be assumed that water passes through similar numbers of bifurcations in the middle reach. In the MTDA and river discharge relation, the ratio of MTDA to river discharge scales with bifurcation order ϕ:

$$\frac{P}{Q_R} \sim \varphi \tag{11}$$

And Eq. (8) can be rewritten as follows:

$$A = \alpha[(\varphi + 1)Q_R]^\beta \tag{12}$$

Figure 10 shows log-log plots of the cross-sectional area A and the discharge conveyed by the channel using (a) river discharge Q_R, (b) the maximum tidal discharge amplitude P, (c) the total discharge $Q_R + P$, and (d) the river discharge scaled with the bifurcation order $\phi + 1$. The relation between A and Q_R shows a larger spreading and reduced slope when compared with the relation between A and P (Fig. 10 a and b). The total discharge $Q_R + P$ shows a nearly unambiguous relation with A (Fig. 10c). After multiplying Q_R with $\phi + 1$, we arrive at a similarly clear relation between A and $(\phi + 1)Q_R$ (Fig. 10d). The bifurcation order $\phi + 1$ is defined as the number of bifurcations preceding a particular cross section. The close relation between the exponents found for $Q_R + P$ and $(\phi + 1)Q_R$ (Fig. 10 c and d) suggests that adding the bifurcation order may improve the goodness of fit. This is useful when no observed or simulated tidal characteristics are available.

Fig. 12 The discharge asymmetry index Ψ at the bifurcations of PRD in high flow **a** for simulation forced by river discharge and tide and **b** for simulation forced by river discharge only
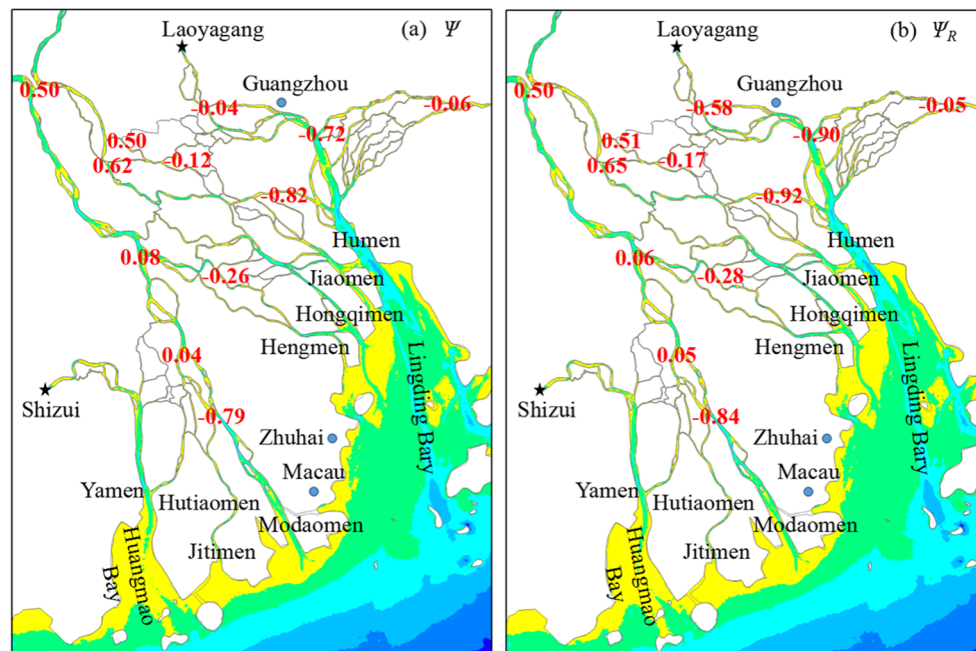
Fig. 13 Spatial distribution of diurnal (D_1; **a**), semidiurnal (D_2; **b**), quarterdiurnal (D_4; **c**), and fortnightly ($D_{1/14}$; **d**) tidal contributions to water surface variation, in meters
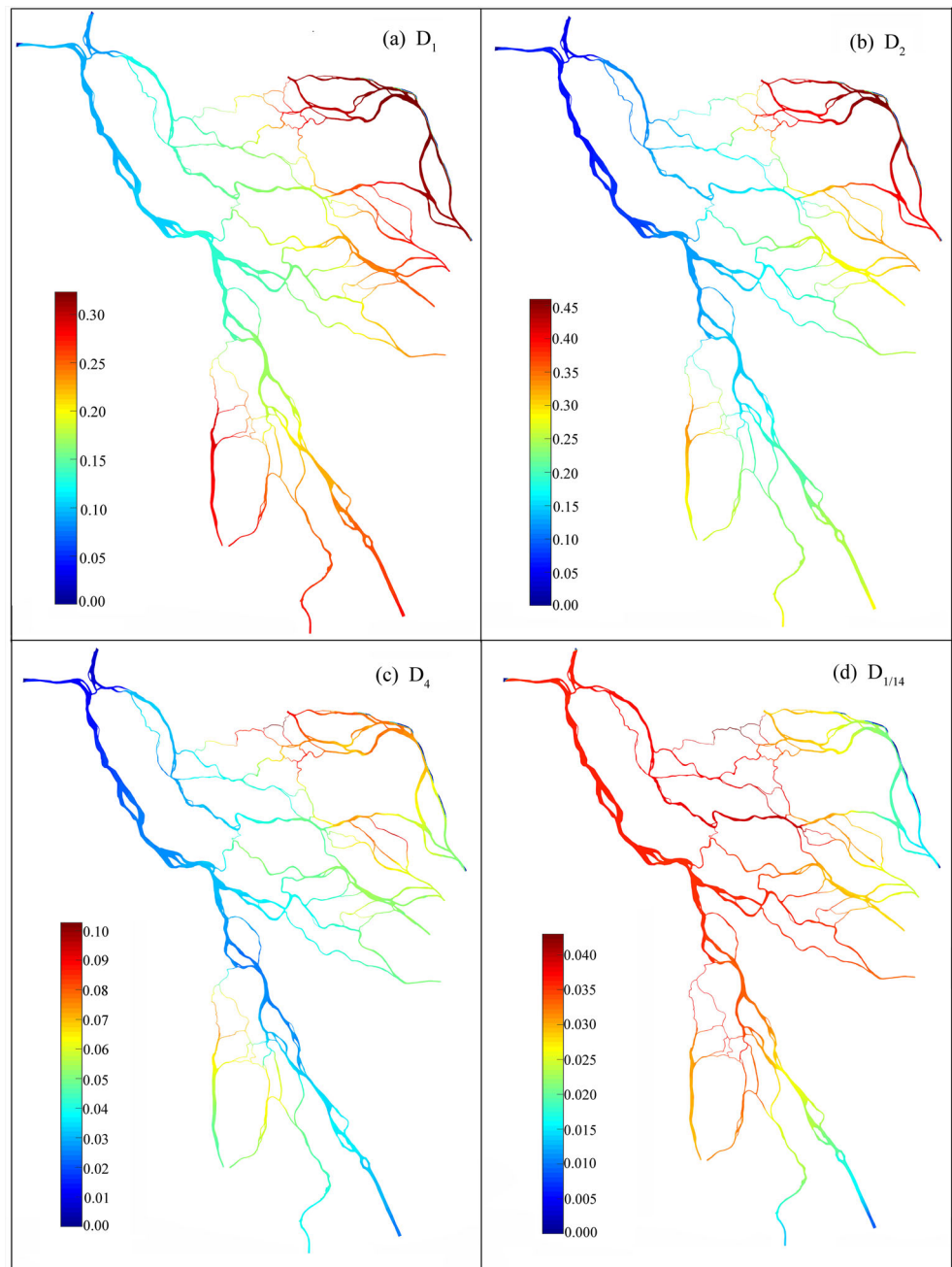

Figure 11 demonstrates the same data as Fig. 10 c and b, for simulations with high flow, but binned and averaged over s/L, and color coded for incremental ranges of s/L. The cross-section area depicts an obvious linear relationship with the total discharge (Fig. 11a), indicating that the impact of total discharge on the channel morphology is generally consistent from the delta apex to the coast. However, there is a transition point at $s/L = 0.6$, which indicates that tidal impact is different in the upper and lower reaches of the delta.

4.3 Tidal impact on discharge division

The discharge division at tidal bifurcations leads to variation of the downstream HG exponents and helps to explain the complexity in downstream HG relations of mixed river-tide dominated deltas.

The discharge asymmetry index Ψ is introduced in this study to describe the subtidal discharge division at a bifurcation (Buschman et al. 2010).

$$\Psi = \frac{Q_w - Q_e}{Q_w + Q_e} \tag{13}$$

where Q represents flow discharge (m^3 s^{-1}), and the subscripts w and e denote the west and east bifurcating channels when approaching the bifurcation while moving downstream, respectively. The value of Ψ ranges between -1 and 1. The higher the absolute value of Ψ is, the more unequal the discharge distribution will be (Sassi et al. 2011).

The discharge asymmetry index at the main bifurcations in the PRD is shown in Fig. 12. Most of the discharge asymmetry index are positive, indicating that the water passes through the west channel at most bifurcations. This is in agreement with the fact that more water discharge into the West River network and pour into the South China Sea mainly through the Modaomen outlet. The absolute values of discharge asymmetry index are generally larger in the river only case than the river and tide forced case (Fig. 12). This indicates that discharge differences between the two channels at a bifurcation are relatively large under the river solely condition, and the discharge asymmetry attenuates due to the contributions from tides and river-tide interaction. It can be concluded that the effect of tides is generally to counteract asymmetry in the river discharge division at the bifurcations in the PRD.
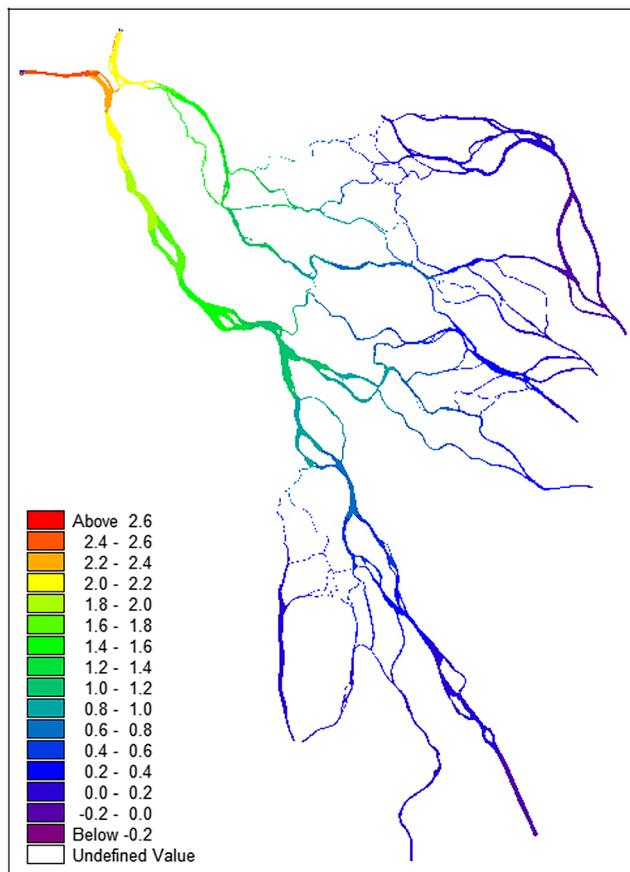

Fig. 14 Spatial distribution of the mean water level in the PRD channel network

At a tidal bifurcation, the water level setup caused by river-tide interaction promotes the allocation of water discharge to the other channel; thus, the differences in water level setup may play an important part in discharge division (Buschman et al. 2010; Sassi et al. 2011). Figure 13 exhibits spatial distributions of the diurnal (D_1), semidiurnal (D_2), quarterdiurnal (D_4), and fortnightly ($D_{1/14}$) contributions to surface level variation, averaged over the entire simulation period. Figure 13 suggests that damping of the main tidal species mostly occurs in the radial direction, showing limited variability across channels along arcs with a constant distance to the delta apex. Only a few (mostly sinuous) channels depict large differences in amplitudes between bifurcating channels.

In general, $D_{1/14}$ amplifies toward the apex, whereas D_1, D_2, and D_4 damp out (Fig. 13). Tidal damping of the main tidal species is generally attributed to frictional forces. Part of the semidiurnal tidal energy is transferred to the overtide and compound tide frequency bands, predominantly via non-linear interaction in the bottom friction term in the momentum balance.

Spatial variations in D_1, D_2, and D_4 resemble each other (Fig. 13a, b, c). D_1 makes the largest contribution in the channels near the Humen and Yamen outlets, especially the Humen outlet which is connected to the Shiziyang tidal channel. D_2 contributes most to the channels near Fubiaochang. In strongly convergent channels, the effects of convergence can surpass the effect of bottom friction, causing tidal amplification (Lanzoni and Seminara 1998). D_2 and D_4 depict relatively large values in several tidal channels and in the sections of distributaries which show to be strongly convergent.

Generally, the contribution of the $D_{1/14}$ is the smallest which is in consistent to the results shown in Fig. 8b. However, the $D_{1/14}$ travels further upstream than D_1, D_2, and D_4 due to the non-linear tidal impact. Figure 14 shows the mean water surface topography averaging over the entire simulation period. Figures 13 d and 14 show good resemblance. $D_{1/14}$ is of great importance to the distribution of the mean water level and thus the discharge division at a bifurcation. It can be regarded as a surrogate for the strength of river-tide interaction (Buschman et al. 2009).

5 Conclusions

Downstream hydraulic geometry (HG) of the distributary channels in the Pearl River Delta (PRD) features distinct characteristics in three zones. The channel width, the cross-sectional area, and the depth to width ratio scale similarly, decreasing from the apex to about 40% of the radial distance, keeping steady within 40~70% of the radial distance, increasing in the remainder of the delta. And the channels become wide and shallow at the eight outlets. The spatial distributions of the mean flow velocity and the ratio of maximum tidal

discharge amplitude (MTDA) to fluvial discharge display similar transitional points.

To quantify the tidal signature on delta morphology, extended hydraulic geometry relations including tides are applied to the channel network in the PRD. The model results of a 2D numerical model are used to analyze the spatial variations of river and tidal discharges and their relations with representative channel geometry throughout the delta. Simulated scenarios include high and low river discharge input, with and without the tidal forcing.

The MTDA quantified by the sum of the mean diurnal, semidiurnal, quarterdiurnal, and fortnightly tidal discharge amplitudes is used instead of the traditional tidal prism. The ratio between MTDA and river discharge scales with bifurcation order since the river discharge reduces as the number of branches increases in the downstream direction. MTDA shows a much closer relation with the cross-sectional area than the river discharge, indicating that the tide plays a decisive role in the formation of the river channel, especially in the seaward portion of the delta.

The non-linear interactions of tidal fluctuation and river discharge create a water level setup which affects the discharge division at tidal bifurcations. In general, the net tidal effect is to attenuate the inequality in discharge division in the PRD. This effect exerts strong impacts on the downstream HG of distributary channels in mixed river-tide-dominated deltas such as the PRD. These results help improve understanding the morphological evolution of delta channel networks subject to tides; applications may be increasingly useful with the ongoing global climatic changes.

References

Allen JI, Somerfield PJ, Gilbert FJ (2007) Quantifying uncertainty in high-resolution coupled hydrodynamic-ecosystem models. J. Mar. Syst 64:3–14. https://doi.org/10.1016/j.jmarsys.2006.02.010

Beaufort A, Moatar F, Curie F, Ducharne A, Bustillo V, Thiéry D (2016) River temperature modelling by Strahler order at the regional scale in the Loire river basin, France. River Res Appl 32:597–609. https://doi.org/10.1002/rra.2888

Braconnot P, Joussaume S, Marti O, de Noblet N (1999) Synergistic feedbacks from ocean and vegetation on the African monsoon response to mid-Holocene insolation. Geophys Res Lett 26:2481–2484. https://doi.org/10.1029/1999GL006047

Buschman FA, Hoitink AJF, Van Der Vegt M, et al (2009) Subtidal water level variation controlled by river flow and tides. Water Resources Research 45(10): W10420, 1–12

Buschman F A, Hoitink A J F, Van Der Vegt M, et al (2010) Subtidal flow division at a shallow tidal junction. Water Resources Research 46(12): W12515, 1–12

Chen XH, Chen YQ (2002) Hydrological change and its causes in the river network of the Pearl River Delta. J Geogr Sci 57:430–436 **(in Chinese)**

Chen X, Zhang W, Zhao H, Xu H, Yi W (2010) Spatio-temporal characteristics and effects of shoreline evolution of the Pearl River estuary in the past thirty years. Trop Geogr 30(6):591–596 **(in Chinese)**

Claussen M, Brovkin V, Ganopolski A (2001) Biogeophysical versus biogeochemical feedbacks of large-scale land cover change. Geophys Res Lett 28:1011–1014. https://doi.org/10.1029/2000GL012471

D'Alpaos A, Lanzoni S, Marani M, Rinaldo A (2010) On the tidal prism-channel area relations. J Geophys Res 115:F01003. https://doi.org/10.1029/2008JF001243

Davies G, Woodroffe CD (2010) Tidal estuary width convergence: theory and form in north Australian estuaries. Earth Surf Process Landf 35(7):737–749

Dodov B, Foufoula-Georgiou E (2004) Generalized hydraulic geometry: insights based on fluvial instability analysis and a physical model. Water Resour Res 40:W12201. https://doi.org/10.1029/2004WR003196

Dupas R, Curie F, Gascuel-Odoux C, Moatar F, Delmas M, Parnaudeau V, Durand P (2013) Assessing N emissions in surface water at the national level: comparison of country-wide vs. regionalized models. Sci Total Environ 443:152–162. https://doi.org/10.1016/j.scitotenv.2012.10.011

Edmonds DA, Slingerland RL (2007) Mechanics of river mouth bar formation: implications for the morphodynamics of delta distributary network. J Geophys Res 112(F02034):1–16

Fagherazzi S, Furbish DJ (2001) On the shape and widening of salt marsh creeks. J Geophys Res 106(C1):991–1003. https://doi.org/10.1029/1999JC000115

Friedrichs CT (1995) Stability shear stress and equilibrium cross-sectional geometry of sheltered tidal channels. J Coastal Res 11(4):1062–1074

Godin G (1985) Modification of river tides by the discharge. Journal of Waterway, Port, Coastal, and Ocean Engineering 111(2):257–274. https://doi.org/10.1061/(ASCE)0733-950X(1985)111:2(257)

Goodwin P (2004) Analytical solutions for estimating effective discharge. J Hydraul Eng 130:729–738. https://doi.org/10.1061/(ASCE)0733-9429(2004)130:8(729)

Hogrefe C et al (2004) Simulating changes in regional air pollution over the eastern United States due to changes in global and regional climate and emissions. J Geophys Res 109:D22301. https://doi.org/10.1029/2004JD004690

Hoitink AJF, Wang ZB, Vermeulen B, Huismans Y, Kästner K (2017) Tidal controls on river delta morphology. Nat Geosci 10:637–645

Jay DA (1997) Interaction of fluctuating river flow with a barotropic tide: a demonstration of wavelet tidal analysis methods. J. Geophys. Res. 102(C3): 5705–5720. 10.1 029/96JC00496

Ji X, Zhang W (2019) Tidal influence on the discharge distribution over the Pearl River Delta, China. Reg Stud Mar Sci 31:100791

Ji X, Sheng J, Tang L, Liu D, Yang X (2011) Process study of circulation in the Pearl River Estuary and adjacent coastal waters in the wet season using a triply-nested circulation model. Ocean Model 28:138–160. https://doi.org/10.1016/j.ocemod.2011.02.010

Jia L, Yang Q, Haiqiang Q, Luo X, Luo Z, Yang G (2002) Variations in At-a-Station hydraulic geometry of the Pearl River Delta in recent decades. Sci Geogr Sin 22(1):57–62

Lamouroux N, Hauer C, Stewardson MJ, LeRoy Poff N (2017) Chapter 13–physical habitat modeling and ecohydrological tools. In: Horne AC, Webb JA, Stewardson MJ, Richter B, Acreman M (Eds.), Water for the Environment. Academic Press, pp. 265–285. https://doi.org/10.1016/B978-0-12-803907-6.00013-9

Langbein WB (1963) The hydraulic geometry of a shallow estuary. Bulletin-International Association of Scientific Hydrology 8(3):84–94. https://doi.org/10.1080/02626666309493340

Lanzoni S, G Seminara (1998) On tide propagation in convergent estuaries, J. Geophys. Res. 103(C13): 30, 793–30, 812. https://doi.org/10.1029/1998JC900015

Lee JS, Julien PY (2006) Downstream hydraulic geometry of alluvial channels. J Hydraul Eng 132:1347–1352. https://doi.org/10.1061/(ASCE)0733-9429(2006)132:12(1347)

Leopold LB, Maddock T (1953) The hydraulic geometry of stream channels and some physiographic implications. U S Geol Surv Prof Pap 252:1–58

Lu XX, Zhang SR, Xie SP, Ma PK (2007) Rapid channel incision of the lower Pearl River (China) since the 1990s. Hydrol Earth Syst Sci Discuss 4:2205–2227

Luo XL, Zeng EY, Ji RY, Wang CP (2007) Effects of in-channel sand excavation on the hydrology of the Pearl River Delta, China. J Hydrol 343:230–239

Maddock I (1999) The importance of physical habitat assessment for evaluating river health. Freshw Biol 41:373–391. https://doi.org/10.1046/j.1365-2427.1999.00437.x

Mao Q, Shi P, Yin K, Gan J, Qi Y (2004) Tides and tidal currents in the Pearl River Estuary. Cont Shelf Res 24(16):1797–1808

Maréchal D (2004) A soil-based approach to rainfall-runoff modelling in ungauged catchments for England and Wales (Ph.D. thesis). Cranfield University

Miguel C, Lamouroux N, Pella H, Labarthe B, Flipo N, Akopian M, Belliard J (2016) Altération d'habitat hydraulique à l'échelle des bassins versants: impacts des prélèvements en nappe du bassin Seine-Normandie. Houille Blanche:65–74 (in French). https://doi.org/10.1051/lhb/2016032

Myrick RM and LB Leopold (1963) Hydraulic geometry of a small tidal estuary. U.S. Dept. Int., Geol. Surv. Prof. Pap. 422–B: 1–18

Nienhuis JH, Hoitink AJF, Törnqvist TE (2018) Future change to tide-influenced deltas Geophysical Research Letters 45. https://doi.org/10.1029/2018GL077638

Pearl River Water Resources Commission (1991) Pearl River records, Volume III. Guangdong Province Science and Technology Press, Guangzhou, China, 256 pp (in Chinese)

Rinaldo A, Fagherazzi S, Lanzoni S, Marani M, Dietrich WE (1999) Tidal networks: 3. Landscape-forming discharges and studies in empirical geomorphic relationships. Water Resour Res 35(12):3919–3929

Sassi MG and AJF Hoitink (2013) River flow controls on tides and tide-mean water level profiles in a tidal freshwater river. J Geophys Res Oceans 118: 4139–4151. https://doi.org/10.1002/jgrc.20297

Sassi MG, Hoitink AJF, de Brye B, Vermeulen B, Deleersnijder E (2011) Tidal impact on the division of river discharge over distributary channels in the Mahakam Delta. Ocean Dyn 61(12):2211–2228

Sassi MG, Hoitink AJF, de Brye B, Deleersnijder E (2012) Downstream hydraulic geometry of a tidally influenced river delta. J Geophys Res 117:F04022. https://doi.org/10.1029/2012JF002448

Savenije HHG (2012) Salinity and tides in alluvial estuaries, 2nd edn. Elsevier, New York

Smagorinsky J (1963) General circulation experiments with the primitive equations, part 1, basic experiment. Monthly Weather Review 91: 99–164. https://doi.org/10.1175/1520-0493(1963)091<0099:GCEWTP>2.3.CO;2

Snelder T, Booker D, Lamouroux N (2011) A method to assess and define environmental flow rules for large jurisdictional regions. J Am Water Resour Assoc 47:828–840. https://doi.org/10.1111/j.1752-1688.2011.00556.x

Statzner B, Gore JA, Resh VH (1988) Hydraulic stream ecology: observed patterns and potential applications. J North Am Benthol Soc 7:307–360. https://doi.org/10.2307/1467296

Stein U, Alpert P (1993) Factor separation in numerical simulations. J Atmos Sci 50(4):2107–2115

Stewardson MJ, Datry T, Lamouroux N, Pell H, Thommeret N, Valette L, Grant SB (2016) Variation in reach-scale hydraulic conductivity of streambeds. Geomorphology 259(15):70–80

Syvitski JPM, Saito Y (2007) Morphodynamics of deltas under the influence of humans. Glob Planet Chang 57(3):261–282

Torma C, Giorgi F (2014) Assessing the contribution of different factors in regional climate model projections using the factor separation method. Atmos Sci Lett 15:239–244. https://doi.org/10.1002/asl2.491

van den Heever SC, Carrio GG, Cotton WR, DeMott PJ, Prenni AJ (2006) Impacts of nucleating aerosol on Florida storms. Part I: mesoscale simulations. J Atmos Sci 63:1752–1775. https://doi.org/10.1175/JAS3713.1

Williams PB, Orr MK, Garrity NJ (2002) Hydraulic geometry: a geomorphic design tool for tidal marsh channel evolution in wetland restoration projects. Restor Ecol 10(3):577–590

Wright LD, Coleman JM, Thom BG (1973) Processes of channel development in a high-tide-range environment: Cambridge Gulf-Ord River Delta, Western Australia. J Geol 81(1):15–41. https://doi.org/10.1086/627805

Yuan R, Zhu J (2015) The effects of dredging on tidal range and saltwater intrusion in the Pearl River estuary. J Coast Res 31(6):1357–1362

Zhang W, Xiaohong R, Zheng J, Zhu Y, Wu H (2010) Long-term change in tidal dynamics and its cause in the Pearl River Delta, China. Geomorphology 120(3–4):209–223

Zhang W, Wang W, Zheng J, Wang H, Wang G, Zhang J (2015) Reconstruction of stage-discharge relationships and analysis of hydraulic geometry variations: the case study of the Pearl River Delta, China. Glob Planet Chang 125:60–70

Zhang W, Feng HC, Hoitink AJF, Zhu YL, Gong F, Zheng JH (2017) Tidal impacts on the subtidal flow division at the main bifurcation in the Yangtze River Delta. Estuar. Coast Shelf Sci. 196: 301–314. /https://doi.org/10.1016/j.ecss.2017.07.008

Zhao HT (1990) Evolution of the Pearl River Estuary. Chinese Ocean Press, Beijing, p 357 (in Chinese)